The 4th International Conference on
Advances in Wind and Structures(AWAS'08)
Jeju, Korea, May 29-31, 2008

Galloping response prediction of ice-accreted transmission lines

Muhammad Bilal Waris[1)]*, Takashi Ishihara[2)], Muhammad Waheed Sarwar[3)]

[1), 2), 3)] *Institute of Engineering Innovation, School of Engineering, University of Tokyo, 2-11-16, Yayoi, Bunkyo-ku, Tokyo 113-8656, Japan*
[1)] *waris@bridge.t.u-tokyo.ac.jp*

ABSTRACT

Transmission lines are extremely flexible structures, which can suffer from galloping under extreme environmental conditions. A better understanding of the phenomena is therefore necessary to predict occurrence and extent of this phenomenon. In this study, an aero-elastic experiment has been performed on sectional model of four-conductor transmission line considering different structural configurations. The experiment is reproduced numerically using a nonlinear FEM code, in which aerodynamic force is estimated using quasi-steady and unsteady force model. Dependence of galloping on structural configuration and efficiency of aerodynamic force prediction models is investigated in light of experiment and simulation results.

1. INTRODUCTION

Transmission lines that vary from supply to local feeders to countrywide supply to remote areas are essential part of every country's development. These are extremely flexible structures and suffer from various types of structural instabilities. The basic concern of this research is "Galloping", which refers to large amplitude oscillation in direction perpendicular to the applied load. During winter, ice accretion takes place on transmission lines, changing their shape, as shown in Figure 1. The modified shape develops aerodynamic lift and rotational moment, which can result in negative aerodynamic damping and lead to galloping. To investigate the galloping phenomena, wind tunnel tests are usually carried out to determine the aerodynamic coefficients as a function of angle of attack. The well-known Den-Hartog criterion is employed considering aerodynamic coefficients to evaluate the possibility of galloping occurrence and critical velocity of galloping for a given cable shape.

---

[1] Graduate Student

[2] Professor

[3] Research Fellow

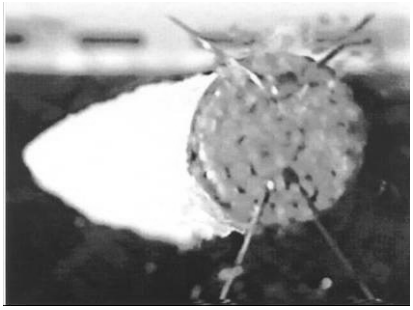

Figure 1 Ice-accretion on cables during winter

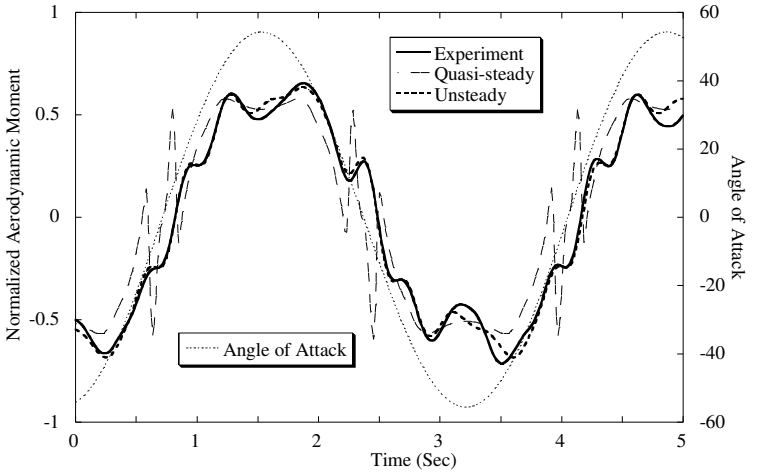

Figure 2 Normalized Aerodynamic Moment considering different Aerodynamic force models (Phuc, 2004)

In most of the previous works galloping of transmission lines has been regarded as a quasi-steady problem. In the last decade, some innovative studies have been carried out to determine influence of conductor motion and conductor wake on the aerodynamic characteristics of transmission lines considering single and 4-conductor bundle ice-accreted cable model (Kimura et al. 1999, Shimizu et al. 2004 and Phuc et. al. 2004). These references put forth a model for representation of unsteady aerodynamic forces considering angle of attack and rotational velocity of cable to take into account the effect of cable motion. The results show that quasi-steady model provide much different results as compared to unsteady model especially for aerodynamic moment (Phuc et al. 2004) as is evident in Figure 2. The figure shows time history of aerodynamic moment on a cable rotating at amplitude of ±55° with respect to steady wind. The unsteady model show very close agreement, whereas the quasi-steady model shows much different results, especially close to 0°.Shimizu and Sato (2001) have used simulation considering quasi-steady model and compared with field observations, some underestimations were observed in the results. The reason of this difference may be because of the difference between the quasi-steady and unsteady aerodynamic coefficients (from Phuc et al. and Shimizu et al.), which is more distinguished for the moment coefficient.

This paper aims to develop a better understanding of galloping phenomena through an aero-elastic experiment. It investigates performance of the aerodynamic force models (quasi-steady and unsteady model) through a fully nonlinear FEM code considering the model for the aero-elastic experiment. Simulation results are used to explain the galloping phenomena.

2. AERO-ELASTIC EXPERIMENT

2.1. Experimental Setup

The aero-elastic experiment is performed in the wind-engineering laboratory of the Department of Civil engineering, The University of Tokyo. It is a vertical closed-circuit type semi open test section wind tunnel with a working section of 16m×1.9m×5.8m (W×H×L) with a contraction ratio of 1/4.2.The maximum wind speed is 17 m/sec.

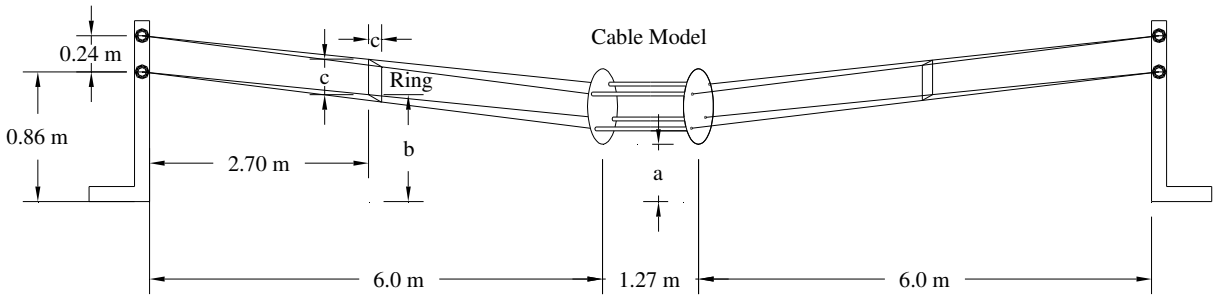

Figure 3 Setup for the Aero-elastic Experiment

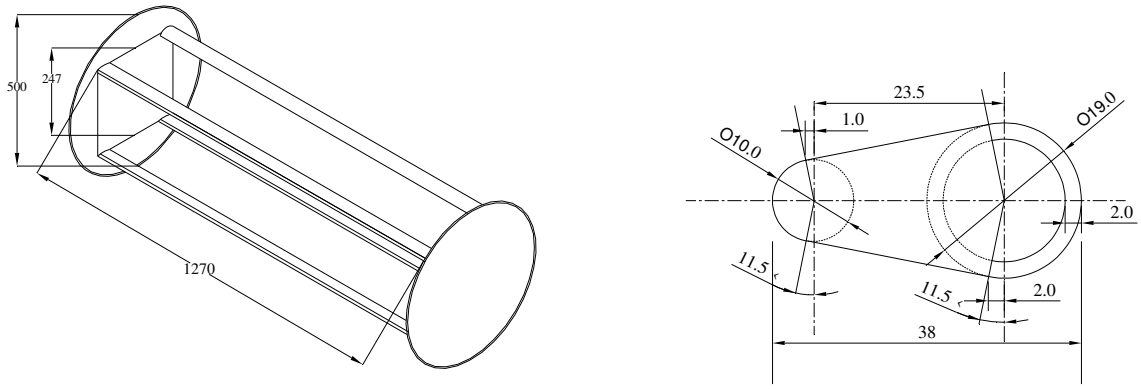

(a) Cable Model (dimension in 'mm') (b) Single Cable Section (mm)

Figure 4 Detail of cable model used in experiment

Table 1 Cases evaluated in the aero-elastic experiment

	Dimension (mm)		
	a	b	c
Case-I	*320*	*660*	*90*
Case-II	*380*	*740*	*0*

The experiment setup is as shown in Figure 3, the cable model is hung from supports through hanger wires 2 mm in diameter. In order to consider cases with different natural frequencies in the experiment, a square-bracing ring is provided on the hanger cables. The size of this ring can be changed to obtain different rotational stiffness. Two ring sizes are considered. The dimensions a, b and c in Figure 1 for the two experiment cases are given in Table 1.

Figure 2 shows details of cable model, the model is 1/3 scale, made of aluminum and wood. The characteristic dimension $B = 247\,mm$ and projected area is $48260\,mm^2$. The experiment is

carried out in uniform-steady wind for increasing and decreasing wind speeds from 5-15 m/sec. The response observations are made at 5 m/sec and then 7-10 m/sec at an interval of 1 m/sec and from 10-15 m/sec at an interval of 0.5 m/sec. The sampling time is 120 sec at a frequency of 30 Hz using a CCD camera. Free vibration is employed to estimate the natural frequency and damping of the system in horizontal, vertical and rotational modes. Results the free vibration are listed in Table 2.

Table 2 Structural parameters for Experiment cases

	Natural Frequency (Hz)			Damping Ratio (%)		
	Horizontal	Vertical	Rotation	Horizontal	Vertical	Rotation
Case-I	*0.70*	*2.55*	*1.40*	*0.30*	*4.20*	*2.60*
Case-II	*0.75*	*2.40*	*0.85*	*4.40*	*5.00*	*4.20*

2.2. Mean Response

Figure 5 shows mean horizontal, vertical and Rotational displacement for the two cases considered in experiment. The mean response before galloping is quite similar for the two cases, but after galloping case-II (with synchronized frequencies) shows greater horizontal and vertical displacement. While mean rotation is nearly same, the vertical displacement in case-II is 2~2.5 times compared with case-I. Further, considering critical velocity for galloping in the two cases, its value should be smaller for case-I with low mechanical damping (Table 2). However, results show opposite tendency with galloping taking place at 11.5 m/sec for case-II compared to 12.5 m/sec for case-I. Such behaviour is observed in case-II because of frequency coupling that amplifies the model response. This influence can also be observed before galloping, as response is greater for case-II, which cause the system to develop negative aerodynamic damping and start galloping at a velocity smaller than anticipated. This idea shall be further explained in section 4.2 with the help of simulation results.

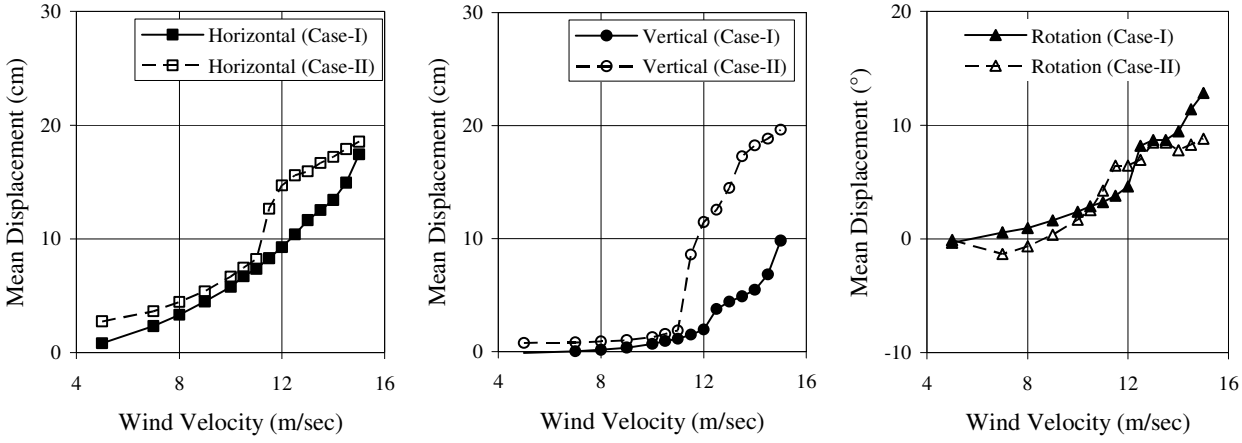

(a) Horizontal (b) Vertical (c) Rotation

Figure 5 Mean response from the aero-elastic experiment

3. NUMERICAL MODELING

3.1. FEM Code

The general information about the numerical code is provided in Table 1. The numerical code has been verified for static, Eigen-value and dynamic solution through comparison with ABAQUS, where as the quasi-steady model for aerodynamic force is validated with CAFSS.

Table 3 Basic Details of the FEM Code

Dynamic analysis	:	Direct implicit integration, Newmark-β method
Eigen-value solution	:	Subspace
Element	:	Beam, Truss, Cable
Formulation	:	Updated Lagrange
Aerodynamic force Model	:	① Quasi-steady theory ② Unsteady theory
Damping	:	Rayleigh damping

3.2. Nonlinear Structural Modeling

The equation of motion can be written in matrix form as:

$$[M]\{\ddot{X}\}+[C]\{\dot{X}\}+[K]\{X\}=\{F\} \tag{1}$$

Where $[M],[C],[K]$ are the mass, damping and stiffness matrices and $\{\ddot{X}\},\{\dot{X}\},\{X\}$ and $\{F\}$ are acceleration, velocity, displacement and external force vectors. The stiffness $[K]$ is:

$$[K]=[K]_E+[K]_T=\left[[K]_E+[K]_{T_o}\right]+[K]_{dT}=[K]_L+[K]_{NL} \tag{2}$$

Where $[K]_E$ is material stiffness, $[K]_T$ is stiffness due to tension. Subscripts 'T_o' and 'dT' represent due to initial tension and fluctuation in tension, $[K]_{T_o}$ and $[K]_{dT}$ represent the corresponding stiffness. Therefore, the total stiffness can be divided into parts; $[K]_L$ is the linear part which is sum of material stiffness $[K]_E$ and stiffness due to initial tension $[K]_{T_o}$, and $[K]_{NL}$ is the nonlinear part which is contribution from variation in element strain to its stiffness.

3.3. Aerodynamic Force Model

Considering Figure 6, the aerodynamic forces acting on a cable model can be given as:

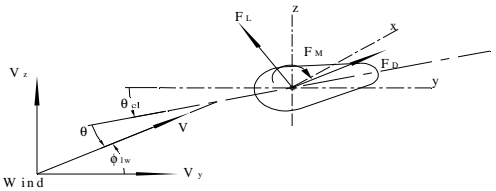

Figure 6 Aerodynamic Force Definition

$$F_D=\frac{1}{2}\rho_a AV^2.C_D$$
$$F_L=\frac{1}{2}\rho_a AV^2.C_L \tag{3}$$
$$F_M=\frac{1}{2}\rho_a A^2V^2.C_M$$

Where F_D, F_L, F_M are aerodynamic drag, lift and moment force respectively, 'ρ_a' is air density, 'A' is characteristic projected area and 'V' is the mean wind velocity. The aerodynamic coefficients C_D, C_L, C_M are a function of angle of attack 'θ' in quasi-steady approximation $\{C_{D,L,M}(\theta)\}$, whereas in unsteady approximation they are derived considering angle of attack 'θ' and element rotational velocity '$\dot{\theta}_{el}$'. The aerodynamic force is estimated considering the quasi-steady and unsteady model from the data available from (Phuc et al 2004) as given in Figure 7. This implies that aerodynamic force on the cable element is dependent only on angle of attack in quasi-steady model, whereas it is evaluated based on angle of attack and element rotational velocity.

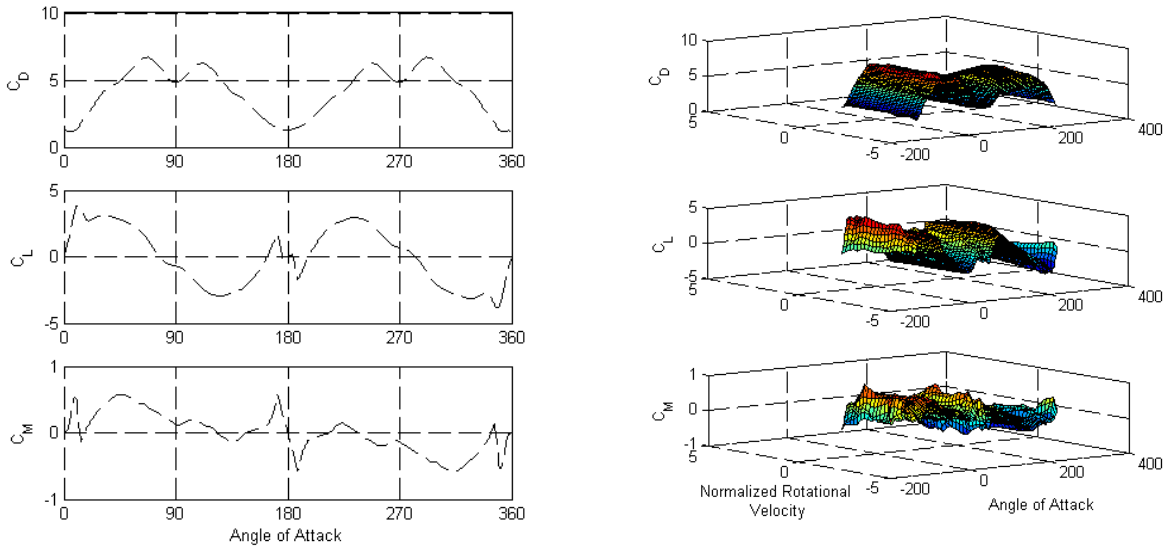

(a) Quasi-steady Model (b) Unsteady Model

Figure 7 Aerodynamic coefficients for the 4-conductor cable model (Phuc et al 2004).

4. NUMERICAL MODEL FOR AEROELASTIC EXPERIMENT

The material and sectional properties of the model are summarized in Table 4.

Table 4 Material and sectional properties of the cable model

Description	Hanger Cable	Cable Model	
		End Plate	Accreted Cable
E (N/m^2)	$3.50\times10^{+10}$	$2.00\times10^{+11}$	$2.00\times10^{+11}$
Density (kg/m^3)	2000	- -	- -
Weight (kg)	0.307	4.09	
Diameter (m)	0.002	0.020	0.019
Cross-sectional Area(m^2)	3.14×10^{-06}	3.14×10^{-04}	2.84×10^{-04}
Moment of Inertia (m^4)	7.85×10^{-13}	7.85×10^{-09}	6.40×10^{-04}
Polar moment of inertia (m^4)	1.57×10^{-12}	1.57×10^{-08}	1.28×10^{-08}

The numerical model of the aero-elastic model is developed considering the equivalence of natural frequency. For numerical model the whole cable model is divided into two components, the hanger wires which are modeled as “Truss” and the cable model itself is modeled as “Beam”.

4.1. Free Vibration

In order to check the numerical model, free vibration of the model is simulated to evaluate natural frequency and structural damping in horizontal (lateral), vertical and torsional modes. Comparison of frequency analysis from free vibration is shown in Figure 8 and Table 5.

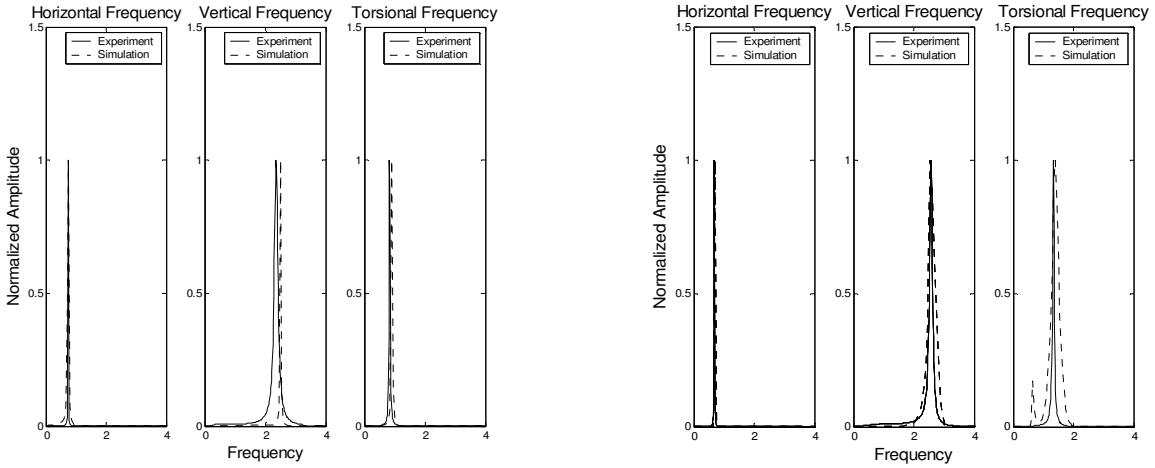

(a) Case-I (b) Case-II

Figure 8 Structural frequencies of the aero-elastic experiment model

Table 5 Comparison of Structural Frequency and damping from experiment and simulation

		Horizontal			Vertical			Torsional		
		Sim.	Exp.	Diff. (%)	Sim.	Exp.	Diff. (%)	Sim.	Exp.	Diff. (%)
Frequency	Case-I	*0.70*	*0.70*	*0.0*	*2.50*	*2.55*	*-2.0*	*1.40*	*1.35*	*3.7*
	Case-II	*0.75*	*0.75*	*0.0*	*2.50*	*2.35*	*6.4*	*0.85*	*0.90*	*-5.5*
Damping	Case-I	*0.030*	*0.030*	*0.0*	*0.042*	*0.042*	*0.0*	*0.025*	*0.026*	*-3.8*
	Case-II	*0.045*	*0.044*	*2.3*	*0.048*	*0.050*	*-4.0*	*0.043*	*0.042*	*2.4*

The numerical model provides acceptable result for both damping and natural frequency, with maximum difference in frequency of 6.4 % and damping of 4.0 % for the vertical DOF. The difference is considered to be because of two factors. First is contact friction between the cable model and hanger wire and that between square ring and hanger wire, and the other is pre-tension in the hanger wire due to presence of square ring. As these two factors are more dominant in case-II, the difference is greater for the said case. However, as their influence is not significant, they are not included in the current model.

4.2. Aero-elastic Experiment

The simulation considering the experiment conditions was carried out using a time step of 0.001 sec, the data considered in evaluating the mean and standard deviation has a time elapse of 120 sec (similar to experiment). As in the experiment, simulation is also carried out in similar wind velocity cycle. Acceleration between velocities is kept small enough to avoid impact. Standard deviation of horizontal (lateral), vertical and rotational response for the two cases is shown in Figure 9 and Figure 10 along with simulation results.

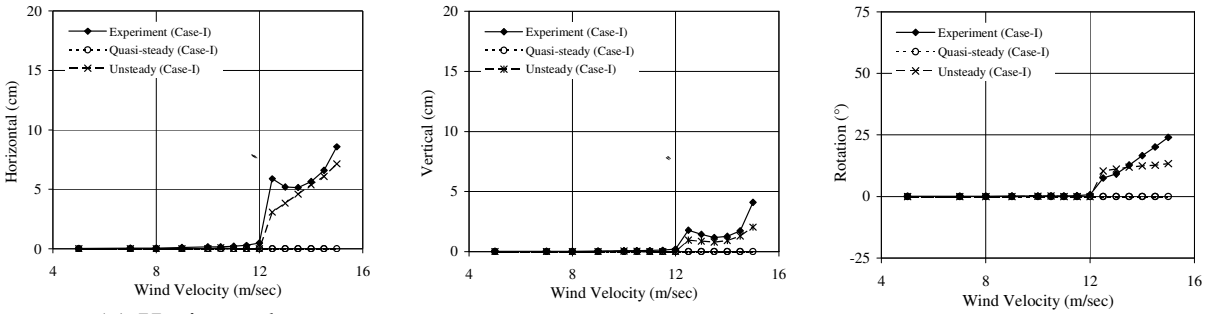

(a) Horizontal (b) Vertical (c) Rotational

Figure 9 Comparison of Quasi-steady and unsteady simulation with experiment (Case-I)

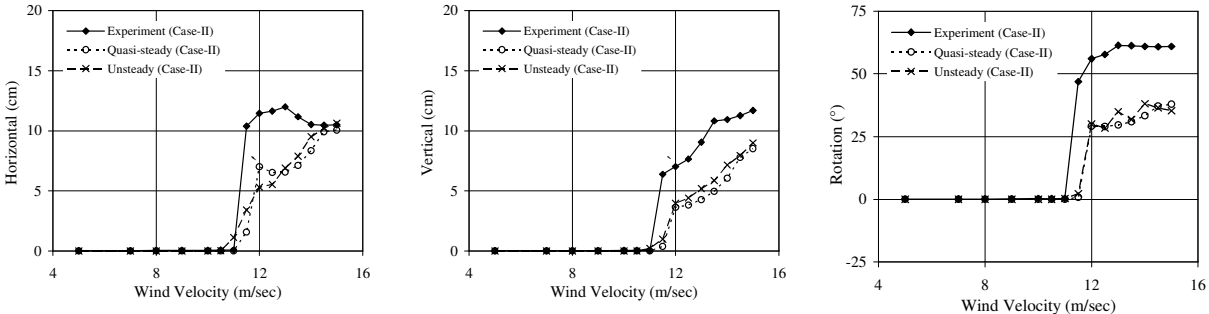

(a) Horizontal (b) Vertical (c) Rotational

Figure 10 Comparison of Quasi-steady and unsteady simulation with experiment (Case-II)

Figure 9 indicates that the quasi-steady theory is unable to predict the occurrence of galloping in case-I, whereas unsteady theory shows acceptable agreement. Figure 11 shows time history for the wind velocity 'U', the angle of attack 'θ', normalized rotational velocity '$B\dot{\theta}_{el}/U$' (where 'B' is characteristic dimension, '$\dot{\theta}_{el}$' element rotational velocity), the aerodynamic moment coefficient 'C_M' and structural damping which is sum of mechanical damping and aerodynamic damping evaluated as in equation below.

$$c = 2m\zeta\omega_1 + \frac{\rho DU}{2}\left(C_D + \frac{dC_L}{d\theta}\right) \tag{4}$$

Only a small portion of the time history is considered, when wind velocity change from 12 m/sec to 12.5 m/sec. Figure 11 (a) it can be seen that quasi-steady model is not able to capitalize on the instability used by variation in wind velocity, as it does not account for the rotational velocity of the model. It does not capture influence of cable motion on the aerodynamic moment and the system returns to stable state at the new wind velocity. On the other hand, in Figure 11 (b) the unsteady force model also includes the effect of reduced rotational velocity $B\dot{\theta}_{el}/U$, where B is the characteristic dimension. Therefore, this model is able to capture the variation in aerodynamic moment. This aerodynamic moment is of significance as it in turn changes the drag and lift forces causing negative aerodynamic damping and resulting in galloping.

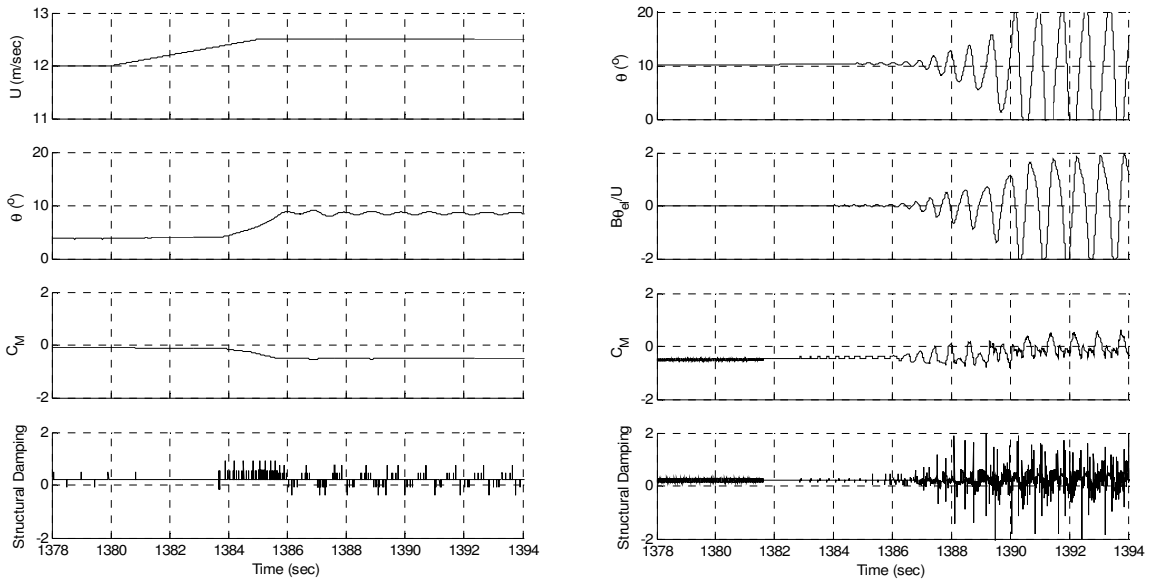

(a) Quasi-Steady Simulation (b) Unsteady Simulation

Figure 11 Hartog criterion for galloping

In case-II (Figure 10), both models show quite similar results, but underestimate the amplitude in comparison with experiment. This result is in accordance with results of Shimizu and Sato (2001). In case-II frequency coupling cause larger displacement, leading to major variation in angle of attack and thus the aerodynamic force. These variation, lead to negative aerodynamic damping and cause galloping.

5. CONCLUSION

An aero-elastic experiment has been performed on a four-conductor cable model. The results indicate that galloping amplitude is higher in system with synchronized frequencies. The critical velocity may also be overestimated using Don-Hartog's principal. Further, the efficiency of aerodynamic models has been investigated using nonlinear 3D-FEM simulations. Comparison of quasi-steady and unsteady aerodynamic force model is provided considering the aero-elastic experiment. Unsteady model is found to provide better results as compared to quasi-steady model for case-I (system with dispersed frequencies), whereas they show similar results for

case-II (coupled frequencies). This means that unsteady model can be considered more robust in predicting occurrence of galloping but is not much better in predicting its amplitude.

REFERENCE

Kimura, K., Inoue, M., Fujino, Y., Yukino, T., Inoue, H., Morishima, H. (1999), "Unsteady forces on an ice-accreted four conductor bundle transmission line", 467-472, ISBN 90 5809 059 0.

Phuc, P.V., Ishihara, T., Shimizu, M. (2004), "A wind tunnel study on unsteady forces of ice-accreted transmission lines", Proc. of BBAA5, July 11-15, Ottawa, Ontario.

Shimizu, M., Ishihara, T., Phuc, P.V. (2004), "A wind tunnel study on aerodynamic characteristics of ice-accreted transmission lines", Proc. of BBAA5, July 11-15, Ottawa, Ontario.

Shimizu, M., Sato, J. (2001), "Galloping observation and simulation of a 4-conductor bundle transmission lines", J. Str. Eng., Vol. 47A, 479 – 488, 2001. (in Japanese).